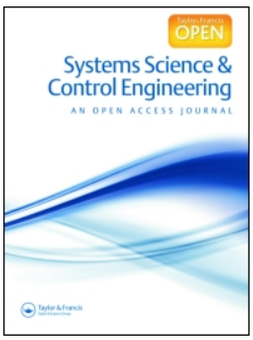

Systems Science & Control Engineering

An Open Access Journal

ISSN: (Print) 2164-2583 (Online) Journal homepage: https://www.tandfonline.com/loi/tssc20

Trajectory tracking control for a quadrotor UAV via extended state observer

Wendong Gai, Jie Liu, Chengzhi Qu & Jing Zhang

To cite this article: Wendong Gai, Jie Liu, Chengzhi Qu & Jing Zhang (2018) Trajectory tracking control for a quadrotor UAV via extended state observer, Systems Science & Control Engineering, 6:3, 126-135, DOI: 10.1080/21642583.2018.1539931

To link to this article: https://doi.org/10.1080/21642583.2018.1539931

Published online: 01 Nov 2018.

SYSTEMS SCIENCE & CONTROL ENGINEERING: AN OPEN ACCESS JOURNAL
2018, VOL. 6, NO. 3, 126–135
https://doi.org/10.1080/21642583.2018.1539931

Taylor & Francis
Taylor & Francis Group

Trajectory tracking control for a quadrotor UAV via extended state observer

Wendong Gai, Jie Liu, Chengzhi Qu and Jing Zhang

College of Electrical Engineering and Automation, Shandong University of Science and Technology, Qingdao, People's Republic of China

ABSTRACT

In this paper, the PD-type trajectory tracking controllevnr with the extended state observer (ESO) is proposed for the quadrotor unmanned aerial vehicle (UAV) to deal with the wind disturbance. A six-degree-of-freedom quadrotor UAV model with the hyperbolic tangent saturation function is built. The trajectory tracking problem for the quadrotor can be divided into the position and attitude loop. Then, the PD-type trajectory tracking controller with the ESO is designed in the position and attitude loop to compensate the effect of the wind disturbance. And the stability of the system is proved by the circle criterion. Simulation results are given to demonstrate the effectiveness of the proposed method.

ARTICLE HISTORY
Received 27 June 2018
Accepted 21 October 2018

KEYWORDS
Proportional-derivative controller; extended state observer; quadrotor unmanned aerial vehicle; trajectory tracking controller

1. Introduction

Recently, as the small unmanned aerial vehicle (UAV) family (Chen, Jiang, Zhang, Jiang, & Tao, 2016), the quadrotor UAV is becoming a popular topic among researchers and scholars because of its vertical takeoff and landing, autonomous hovering and so on (Derafa, Benallegue, & Fridman, 2012; Mandel & Weiss, 2015). Additionally, it has been extensively used in several important applications such as military surveillance, rescue mission, agricultural mapping, and disaster monitoring (Bolandi, Rezaei, Mohsenipour, Nemati, & Smailzadeh, 2013; Fernando, Chandiramani, Lee, & Gutierrez, 2011; Lin, Cai, Wang, Yang, & Chen, 2014). However, it is difficult to control a quadrotor UAV for it is difficult for a quadrotor UAV to finish the attitude and position trajectory tracking when the external disturbance and input saturation constraint are considered (Derafa, Ouldali, Madani, & Benallegue, 2011; Jian & Zhao, 2015; Kerma, Mokhtari, Abdelaziz, & Orlov, 2012; Sheng, Zhang, & Gao, 2014). What's more, how to develop an effective robust flight controller that performs well in practice and ensuring asymptotic stability, in theory, are still a significant challenge because of the external disturbance (Chen, Tao, & Jiang, 2015; Wang, Wang, Bu, Luo, & Tan, 2016).

In the past few years, a large number of literatures have been presented by the researchers around the world for the quadrotor UAV control problem. An ordinary proportional-derivative control and a disturbance compensation control scheme was proposed for quadrotor UAV in Sandiwan, Cahyadi, and Herdjunanto (2017), to compensate unknown external disturbance. However, the object is a 3-DOF model quadrotor UAV system, and it cannot be used in position tracking control. A generalized PI control with adaptively adjusting gains was presented in Song, Wang, and Wen (2016). It can dynamically maintain pre-specified transient and steady-state performance. In Wang, Chen, Sun, and Zhang (2016), an active disturbance rejection control (ADRC) and PID based control method was proposed to finish position and attitude control of a small unmanned quadrotor helicopter model. Nevertheless, the stability analysis is not given in theory.

In addition, the quadrotor UAV inevitably suffers various external disturbance in the practical flight (Chen, Lei, Zhang, Tao, & Jiang, 2016; Mi et al., 2016; Wang, Li, & Guo, 2014). And the wind disturbance is the most serious for the quadrotor UAV. To overcome the disturbance effect, a number of methods are proposed. In Dong, Gu, Zhu, and Ding (2014), a high-performance flight controller with a disturbance observer (DOB) was proposed for trajectory tracking of a quadrotor with external disturbance. The DOB that serves as a compensator is incorporated with backstepping technique. In Li, Jing, Macdonald, and Mcinnes (2011), an adaptive backstepping control law was proposed to track the optimal descent orbit and attitude trajectories. It is shown that this control law is robust against the input saturation and unknown bounded disturbance. However, these techniques based on DOB are only available in the presence of full-state measurements. In Shao, Liu, Cao, Shen, and Wang (2018),

CONTACT Jing Zhang zjing133@sdust.edu.cn

the extended state observers extended state observer (ESO) were constructed to online estimate the unmeasurable velocity states and lumped disturbance existed in translational and rotational dynamics, respectively. Nevertheless, the backstepping controller is more complicated than PD controller for the quadrotor UAV. In this paper, a PD-type control method with ESO is proposed for the quadrotor UAV. The main contributions of this paper are summarized as follows:

(1) The PD-type trajectory tracking control method with the ESO is developed to deal with the wind disturbance. And the stability of the system is proved by the circle criterion.
(2) A six-degree-of-freedom quadrotor UAV model with the hyperbolic tangent saturation function is used in the simulation.

The structure of this paper is organized as follows: Section 2 presents the quadrotor UAV model. In Section 3, the PD-type trajectory tracking controller with ESO is designed, and the stability condition of the system is given using the circle criterion. Next, the numerical simulation and analysis are presented in Section 4. Finally, this paper is concluded in Section 5.

2. The quadrotor UAV modelling

In this section, the quadrotor UAV model is established. The UAV is X layout. And it is a rigid body when the flexible of the mechanical structure is neglected. Its movement can be divided into spatial translational motion and rotation motion. The model of the quadrotor UAV can be written as

$$\begin{cases} \ddot{x} = u_1(\cos\phi\sin\theta\cos\psi + \sin\phi\sin\psi) - K_1\dot{x}/m \\ \ddot{y} = u_1(\sin\phi\sin\theta\sin\psi - \sin\phi\cos\psi) - K_2\dot{y}/m \\ \ddot{z} = u_1(\cos\phi\cos\theta) - g - K_3\dot{z}/m \\ \ddot{\phi} = u_2 - lK_4\dot{\phi}/I_x \\ \ddot{\theta} = u_3 - lK_5\dot{\theta}/I_y \\ \ddot{\psi} = u_4 - lK_6\dot{\psi}/I_z \end{cases} \tag{1}$$

where K_i and m are drag coefficient and mass of the UAV, respectively. x, y, z, ϕ, θ, ψ and $\dot{\phi}, \dot{\theta}, \dot{\psi}$ are the displacement, attitude angle and angular velocity in three directions of the earth's axes. The three attitude angles are roll angle, yaw angle and pitch angle, respectively. Moreover, the inputs of the system are u_1, u_2, u_3, u_4. I_x, I_y, I_z are the rolling rotational inertia, yawing rotational inertia, and pitching rotational inertia, respectively.

In consideration of input saturation constraint of the system, the input u_i is described by

$$u_i = sat(u_i(t)) = \begin{cases} sign(u_i(t))u_M, & |u_i(t)| \geq u_M \\ u_i(t), & |u_i(t)| < u_M \end{cases} \tag{2}$$

where u_i denotes the plant input subject to saturation type nonlinearity. And i can be equal to $1, 2, 3, 4$. u_M is a known bound of u_i. The hyperbolic tangent function is used to deal with the input saturation conveniently. The hyperbolic tangent function can approximate not only the amplitude of the input but also the rate of the input. Furthermore, the hyperbolic tangent function is a smooth curve. And the method can avoid adverse effects of saturation function.

The saturation is approximated by a hyperbolic tangent function defined as

$$g(u_i) = u_M \times \tanh(\frac{u_i}{u_M}) = u_M \frac{e^{u_i/u_M} - e^{-u_i/u_M}}{e^{u_i/u_M} + e^{-u_i/u_M}} \tag{3}$$

Then $sat(u_i)$ in (2) can be expressed as

$$sat(u_i) = g(u_i) + d_1(u_i) \tag{4}$$

Because $sat(u)$ and $g(u)$ are bound function, $d_1(u)$ is bound.

$$|d_1(u)| = |sat(u) - g(u)| \leq u_M(1 - \tanh(1)) \tag{5}$$

Using the Lagrange method, $g(u)$ can be derived by

$$g(u_i) = g(u_i^0) + \frac{\partial g(u_i)}{\partial u_i}|_{u_i = u_i^{\mu_i}}(u_i - u_i^0) \tag{6}$$

where $u_i^{\mu_i} = \mu_i u_i + (1 - \mu_i u_i^0)$, $\mu_i \in (0, 1)$, $i = 1, 2, 3, 4$.

By choosing $u_i^0 = 0$ and considering $g(0) = 0$, we obtain

$$g(u_i) = \frac{\partial g(u_i)}{\partial u_i}|_{u_i = u_i^{\mu_i}} u_i \tag{7}$$

Finally, considering input saturation constraint, the input of the system is

$$u_i = sat(u_i) = g(u_i) + d_1(u_i) \tag{8}$$

Substituting Equation (8) into Equation (1), the quadrotor UAV model can be obtained by

$$\begin{bmatrix} \ddot{x} \\ \ddot{y} \\ \ddot{z} \\ \ddot{\phi} \\ \ddot{\theta} \\ \ddot{\psi} \end{bmatrix} = \begin{bmatrix} sat(u_1)(\cos\phi\sin\theta\cos\psi + \sin\phi\sin\psi) - K_1\dot{x}/m \\ sat(u_1)(\sin\phi\sin\theta\sin\psi - \sin\phi\cos\psi) - K_2\dot{y}/m \\ sat(u_1)(\cos\phi\cos\theta) - g - K_3\dot{z}/m \\ sat(u_2) - lK_4\dot{\phi}/I_x \\ sat(u_3) - lK_5\dot{\theta}/I_y \\ sat(u_4) - lK_6\dot{\psi}/I_z \end{bmatrix} \tag{9}$$

By choosing $U_i = sat(u_i), i = 1, 2, 3, 4$, Equation (9) can be written

$$\begin{bmatrix} \ddot{x} \\ \ddot{y} \\ \ddot{z} \\ \ddot{\phi} \\ \ddot{\theta} \\ \ddot{\psi} \end{bmatrix} = \begin{bmatrix} U_1(\cos\phi\sin\theta\cos\psi + \sin\phi\sin\psi) - K_1\dot{x}/m \\ U_1(\sin\phi\sin\theta\sin\psi - \sin\phi\cos\psi) - K_2\dot{y}/m \\ U_1(\cos\phi\cos\theta) - g - K_3\dot{z}/m \\ U_2 - lK_4\dot{\phi}/I_x \\ U_3 - lK_5\dot{\theta}/I_y \\ U_4 - lK_6\dot{\psi}/I_z \end{bmatrix} \tag{10}$$

In order to verify the accuracy of the model, the simulation data using the built model is compared with the UAV actual flight data. Figure 1 is the actual flying scene of the quadrotor UAV. Taking the pitch angle, for example, the command signal is applied the pitch angle control loop. Then, we can obtain angle and angular velocity response curves in Figures 2 and 3, respectively.

Figure 1. Actual flying scene of the quadrotor UAV.

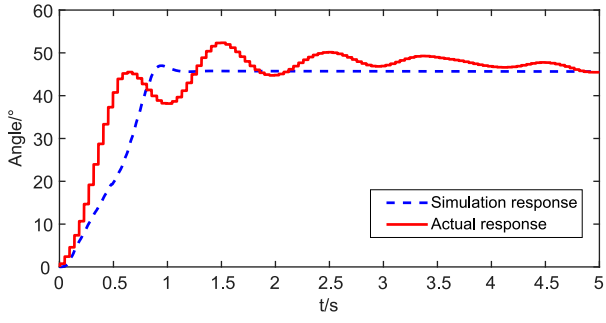

Figure 2. Pitch angle response.

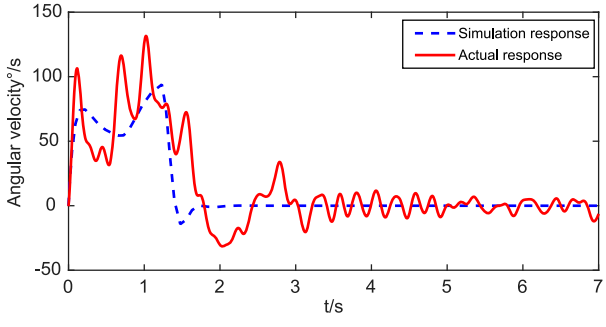

Figure 3. Pitch angular velocity response.

In Figures 2 and 3, the simulation responses are similar to the actual responses. There are fluctuations in the actual responses due to the actual vibration of the frame and the random disturbance from the environment. In response time and trend, it is indicated that the mathematical model can effectively reflect the real situation.

3. PD-type trajectory tracking controller with the ESO

The double loops structure is used in the controller design. The trajectory tracking problem for the quadrotor can be divided into the position loop and attitude loop. The position loop is slow dynamic that it drives the quadrotor to follow the given reference trajectory using the thrust forces. The position loop includes the height subsystem, the *x*-axis subsystem and the *y*-axis subsystem. The attitude loop is fast dynamic that accounts for regulating the orientation to timely track the desired attitude produced by the outer loop. The attitude loop includes the roll subsystem, the pitch subsystem and the yaw subsystem. The roll and pitch angle are gained through virtual input (u_{1x}, u_{1y}) inverse design. In each subsystem, with given information merged into the observer design, a specific linear ESO is constructed to online estimate external disturbance. The control block diagram of ESO trajectory tracking is illustrated in Figure 4. Accurate trajectory tracking performance can be achieved in the absence of velocity information with respect to external disturbance.

3.1. PD-type controller design

Divide the quadrotor model Equation (10) into two parts:

$$\begin{cases} \ddot{x} = U_1(\cos\phi\sin\theta\cos\psi + \sin\phi\sin\psi) - K_1\dot{x}/m \\ \ddot{y} = U_1(\sin\phi\sin\theta\sin\psi - \sin\phi\cos\psi) - K_2\dot{y}/m \\ \ddot{z} = U_1(\cos\phi\cos\theta) - g - K_3\dot{z}/m \end{cases} \tag{11}$$

$$\begin{cases} \ddot{\phi} = U_2 - lK_4\dot{\phi}/I_x \\ \ddot{\theta} = U_3 - lK_5\dot{\theta}/I_y \\ \ddot{\psi} = U_4 - lK_6\dot{\psi}/I_z \end{cases} \tag{12}$$

Equation (11) denotes the position loop of the system model while Equation (12) denotes the attitude loop of the system model.

Define virtual input $u_{1x}u_{1y}u_{1z}$

$$\begin{aligned} u_{1x} &= U_1(\cos\phi\sin\theta\cos\psi + \sin\phi\sin\psi) \\ u_{1y} &= U_1(\cos\phi\sin\theta\sin\psi - \sin\phi\cos\psi) \\ u_{1z} &= U_1(\cos\phi\cos\psi) \end{aligned} \tag{13}$$

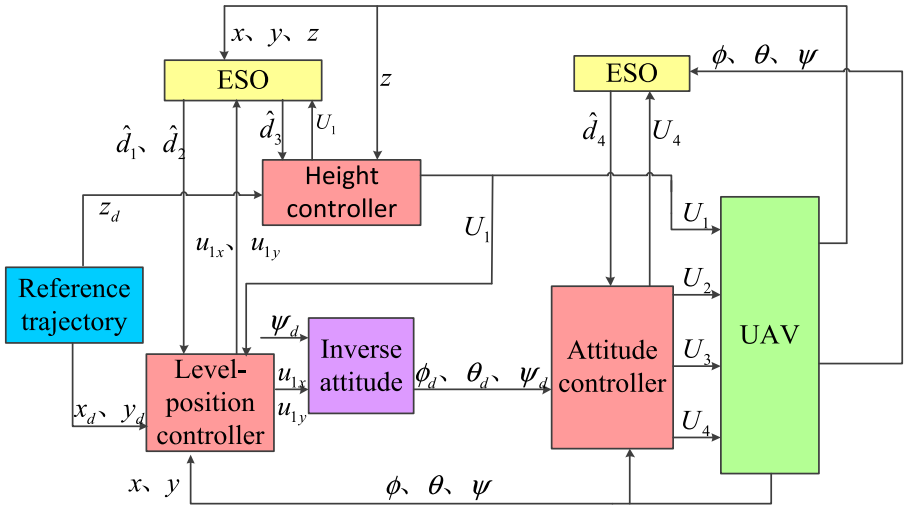

Figure 4. Scheme of trajectory tracking controller of the quadrotor UAV based on PD controller with ESO.

Substituting Equation (13) into Equation (11) yields

$$\begin{cases} \ddot{x} = u_{1x} - K_1\dot{x}/m \\ \ddot{y} = u_{1y} - K_2\dot{y}/m \\ \ddot{z} = u_{1z} - g - K_3\dot{z}/m \end{cases} \tag{14}$$

Take the height subsystem, for example, the output of the PD-type trajectory controller is

$$u_{1z} = -k_{pz}z_e - k_{dz}\dot{z}_e + g + \ddot{z}_0 + \frac{K_3}{m}\dot{z}_0 \tag{15}$$

where $z_e = z - z_0$.

Substituting Equation (15) into the third equation of Equation (14), we can obtain

$$\ddot{z} = -k_{pz}z_e - k_{dz}\dot{z}_e + \ddot{z}_0 - \frac{K_3}{m}\dot{z}_e \tag{16}$$

Namely

$$\ddot{z}_e + (k_{dz} + \frac{K_3}{m})\dot{z}_e + k_{pz}z_e = 0 \tag{17}$$

According to Hurwitz stability theorem of the second-order system, these conditions need to be met as follows

$$\begin{cases} k_{pz} > 0 \\ k_{dz} + \frac{K_3}{m} > 0 \end{cases} \tag{18}$$

Similarly, we can obtain the control input of the *x*, *y*-axis and three attitude angles respectively. The quadrotor position loop control input can be written as

$$\begin{cases} u_{1x} = -k_{px}x_e - k_{dx}\dot{x}_e + \ddot{x}_0 + \frac{K_1}{m}\dot{x}_0 - k_1\hat{d}_1 \\ u_{1y} = -k_{py}y_e - k_{dy}\dot{y}_e + \ddot{y}_0 + \frac{K_2}{m}\dot{y}_0 - k_2\hat{d}_2 \\ u_{1z} = -k_{pz}z_e - k_{dz}\dot{z}_e + g + \ddot{z}_0 + \frac{K_3}{m}\dot{z}_0 - k_3\hat{d}_3 \end{cases} \tag{19}$$

$$\begin{cases} U_2 = -k_{p4}\phi_e - k_{d4}\dot{\phi}_e + \ddot{\phi}_0 + \frac{K_4}{m}\dot{\phi}_0 - k_4\hat{d}_4 \\ U_3 = -k_{p5}\theta_e - k_{d5}\dot{\theta}_e + \ddot{\theta}_0 + \frac{K_5}{m}\dot{\theta}_0 - k_5\hat{d}_5 \\ U_4 = -k_{p6}\psi_e - k_{d6}\dot{\psi}_e + \ddot{\psi}_0 + \frac{K_6}{m}\dot{\psi}_0 - k_6\hat{d}_6 \end{cases} \tag{20}$$

where $\hat{d}_i$ and k_i ($i \in [1, 6]$) are the ESO disturbance estimation and the coefficient of disturbance estimation respectively. $\hat{d}_i$ will be gained through ESO as follow.

3.2. ESO design

In this section, ESO is applied in the position and attitude loops. It is given to offer the disturbance estimation.

Take the height subsystem, for example, the external wind disturbance of the system is estimated and compensated.

Under the influence of wind disturbance, the height subsystem model is

$$\ddot{z} = U_1(\cos\phi\cos\theta) - g - K_3\dot{z}/m + d_3 \tag{21}$$

The system adds a low pass filter to improve the system stability. In Equation (21), $\dot{z}$ is chosen as state x_2, and state x_1 is obtained by

$$x_1 = \frac{1}{\tau s + 1}x_2 \tag{22}$$

The augmented dynamics of the quadrotor height subsystem can be written as

$$\begin{cases} \dot{x}_1 = -\frac{1}{\tau}x_1 + \frac{1}{\tau}x_2 \\ x_2 = -K_3 x_2/m - g + sat(u_1)\cos\phi + d_3 \\ \dot{x}_3 = \dot{d}_3 \\ y = x_1 \end{cases} \tag{23}$$

where d_3 is disturbances of height subsystem, in other word, d_3 is the wind disturbance component in the height direction.

ESO is the core of ADRC and can enhance the anti-disturbance ability of the system (Zhang, Gai, Zhang, & Zhang, 2018). A third-order ESO is designed for the second-order height subsystem model as follows:

$$\begin{cases} e = z_1 - y \\ \dot{z}_1 = -\frac{1}{\tau}z_1 + \frac{1}{\tau}z_2 - \beta_1 fal_1 \\ \dot{z}_2 = -K_3 z_2 + z_3 - \beta_2 fal_2 + (\cos\phi\cos\theta)u_1 - g \\ \dot{z}_3 = -\beta_3 fal_3 \end{cases} \tag{24}$$

where $\beta_i (i = 1, 2, 3)$ is the observer gain and $z_i (i = 1, 2, 3)$ is the output of the ESO which is the estimation of state $x_i (i = 1, 2, 3)$, respectively. Then the ESO can estimate disturbances without the information of $\dot{d}_3(t)$. And $fal_i (i = 1, 2, 3)$ function is defined as

$$fal_i = \begin{cases} e/\delta_i^{1-\alpha_i} & |e| \le \delta_i \\ |e|^{\alpha_i}\mathrm{sgn}(e) & |e| > \delta_i \end{cases} \tag{25}$$

Similarly, we can obtain ESO of other subsystem. Moreover, the stability of the ESO method is analysed as follows.

3.3. The stability analysis

For convenience in analysing the stability of the system, the model of the quadrotor UAV is simplified as a Lurie system.

State error feedback (SEF) is designed as follows

$$\begin{cases} u_0 = k_p(v_1 - z_1) + k_d(v_2 - z_2) \\ u = \frac{u_0 - z_3}{b} \end{cases} \tag{26}$$

where k_p and k_d are the gains of the SEF. b is the gain parameter of control input.

Substituting Equation (26) into Equation (23), we can obtain

$$\begin{cases} \dot{X} = A_{11}X + A_{12}Z + a_{13}z_3 \\ y = x_1 \end{cases} \tag{27}$$

where $X = [x_1, x_2]^{\mathrm{T}}$, $Z = [z_1, z_2]^T$ $a_{\alpha 3} = [0, -\frac{\cos\phi\cos\psi}{b}]^T$, $A_{11} = \begin{bmatrix} -\frac{1}{\tau} & -\frac{1}{\tau} \\ 0 & -\frac{k_3}{m} \end{bmatrix}$ and $A_{12} = \begin{bmatrix} 0 & 0 \\ -\frac{\cos\phi\cos\psi}{b}k_1 & -\frac{\cos\phi\cos\psi}{b}k_2 \end{bmatrix}$.

Substituting Equation (26) into Equation (24) yields

$$\begin{cases} \dot{Z} = A_{21}Z + b_{22}\hat{u}_1 \\ \dot{z}_3 = \beta_3\hat{u}_2 \end{cases} \tag{28}$$

where $\hat{u}_1 = \begin{bmatrix} fal_1 & fal_2 \end{bmatrix}$, $\hat{u}_2 = fal_3$, $b_{22} = [\beta_1, \beta_2]^T$ and $A_{21} = \begin{bmatrix} -\frac{1}{\tau} & -\frac{1}{\tau} \\ -\frac{\cos\phi\cos\psi}{b}k_1 & -\frac{\cos\phi\cos\psi}{b}k_1 \end{bmatrix}$.

Combining the Equation (27) and Equation (28), the system is obtained as

$$\begin{cases} \dot{X} = A_{11}X + A_{12}Z + a_{13}Z_3 \\ \dot{Z} = A_{21}Z + b_{22}\hat{u}_1 \\ Z_3 = \beta_3\hat{u}_2 \\ \sigma = c_1^T X + c_2^T Z \end{cases} \tag{29}$$

where $c_1 = [-1, 0]^T$, $c_2 = [1, 0]^T$.

Set $Y = A_{11}X + a_{13}z_3$, then we get

$$\begin{cases} \dot{Y} = A_{11}X + A_{11}A_{12}Z - \beta_3\hat{u} \\ \dot{Z} = A_{21}Z + b_{22}\hat{u} \\ E = c_1^T A_{11}^{-1}Y + c_2^T Z + A_{11}^{-1}z_3 \end{cases} \tag{30}$$

Set $\hat{X} = [x_1, x_2, z_1, z_2]^{\mathrm{T}}$, then the system (Equation (30)) can be described as a standard Lurie system.

$$\begin{cases} \dot{\hat{X}} = \tilde{A}\hat{X} + \tilde{b}\tilde{u} \\ \dot{\xi} = d_1\tilde{u} \\ \sigma = c^T\hat{X} + \rho\xi \end{cases} \tag{31}$$

where

$$\tilde{A} = \begin{bmatrix} A_{11} & A_{11}A_{12} \\ 0 & A_{21} \end{bmatrix}$$

$$= \begin{bmatrix} -\frac{1}{\tau} & \frac{1}{\tau} & -\frac{\cos\phi\cos\psi}{\tau b}k_1 & -\frac{\cos\phi\cos\psi}{\tau b}k_2 \\ 0 & -\frac{k_3}{m} & \frac{\cos\phi\cos\psi}{mb}k_1k_3 & \frac{\cos\phi\cos\psi}{mb}k_2k_3 \\ 0 & 0 & -\frac{1}{\tau} & \frac{1}{\tau} \\ 0 & 0 & -\frac{\cos\phi\cos\psi}{b}k_1 & -\frac{\cos\phi\cos\psi}{b}k_2 \end{bmatrix},$$

$$\tilde{b} = \begin{bmatrix} -\beta_3 \\ b_{22} \end{bmatrix} = [-\beta_3 \quad \beta_2 \quad \beta_1]^T,$$

$$\tilde{u} = -[fal_3(e, \alpha_3, \delta_3) \quad fal_2(e, \alpha_2, \delta_2) \quad fal_1(e, \alpha_1, \delta_1)],$$

$d_1 = [-1\ 0\ 0]^T$, $\rho = -c_1^T A_{\alpha 1}^{-1}(-\beta_3) = -\tau\beta_3$, and $c = \begin{bmatrix} c_1^T A_{\alpha 1}^{-1} & c_2^T \end{bmatrix}$.

The estimated disturbances z_3 is included in $\dot{\xi}$. Thus, the Lurie system is displayed in Figure 5 (Gan & Han, 2003; Li et al., 2015).

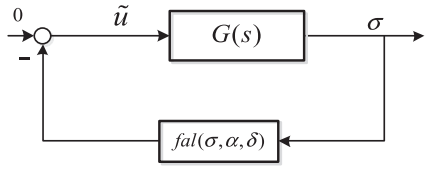

Figure 5. Lurie system.

$G(s)$ is obtained by

$$G(s) = c^T(sI - \tilde{A})^{-1}\tilde{b} + \rho/s \tag{32}$$

The four eigenvalues of $\tilde{A}$ can be derived

$$\begin{cases} \lambda_1 = -1/\tau \\ \lambda_2 = -k_3/m \\ \lambda_3 = -1/\tau \\ \lambda_4 = -k_2\cos\phi\cos\theta/b - b/(k_1\cos\phi\cos\theta) \end{cases}, \tag{33}$$

Due to τ, m, k_1, k_2, k_3 are all positive, and the $\tilde{A}$ is invertible if $\lambda_4 \neq 0$. The stability of the Lurie system is proved by the circle criterion.

Lemma 1: *According to Figure 5, for a zero input, the negative feedback system with a nonlinear, time-varying, nonnegative gain is*

$$\dot{x} = Ax + f(x,t)Bx \tag{34}$$

where $f(x,t) \in [\varphi_1, \varphi_2]$ is a time-varying gain and matrices A and B are expressed as

$$A = \begin{bmatrix} 0 & 1 & \dots & 0 \\ \vdots & \vdots & & \vdots \\ 0 & 0 & \dots & 1 \\ -a_n & -a_{n-1} & \dots & -a_1 \end{bmatrix}, B = \begin{bmatrix} 0 & 0 & \dots & 0 \\ \vdots & \vdots & & \vdots \\ 0 & 0 & \dots & 0 \\ -b_{n-1} & -b_{n-2} & \dots & -b_1 \end{bmatrix},$$

where real numbers $a_1, \dots, a_n$ and $b_1, \dots, b_{n-1}$ are determined by the following relations:

$$q(s) = b_0 s^{n-1} + \cdots + b_{n-1} \tag{35}$$

$$p(s) = s^n + a_1 s^{n-1} + \cdots + a_n \tag{36}$$

This class of differential systems is denoted as D_{φ_1,φ_2}. Every differential system in class D_{φ_1,φ_2} is stable in the large if

(1) *$p(s) + kq(s)$ has no zeroes in the right half-plane* Re *s <0 for any $k \in [\varphi_1, \varphi_2]$*
(2) $\mathrm{Re}[(p(-j\omega) + \varphi_1 q(-j\omega))(p(j\omega) + \varphi_2 q(j\omega))] \geq 0$ $\forall\omega \in R$

Theorem 1: *The nonlinear system in Equation (30) is frozen-time closed-loop stable (asymptotically stable) in interval $J_{t^*} \subseteq [\frac{1}{\varphi_2}, \frac{1}{\varphi_1}]$, if*

$$\lambda_i \leq 0 \tag{37}$$

$$\frac{1}{\varphi_2} \geq -\frac{\mathrm{Re}[G(j\omega)] + \varphi_1|G(j\omega)|^2}{1 + \varphi_1\mathrm{Re}[G(j\omega)]} \forall\omega \in \Omega_\varphi \tag{38}$$

where λ_i ($i = 1, 2 \dots n$) are zeroes of the height subsystem, and $\Omega_\varphi = \Re - \Omega^*_{\varphi'}$, $\Omega^*_\varphi = \{\hat{\omega} : 1 + \varphi_1\mathrm{Re}[G(j\hat{\omega})] = 0$ or $\hat{\omega} = 0\}$.

Proof: When $\alpha < 1$, we obtain

$$\lim_{e\to\infty} e^{\alpha-1} \leq \frac{fal(e) - fal(0)}{e - 0} \leq \delta^{\alpha-1} \tag{39}$$

Substituting $fal(0) = 0$ into Equation (39), Equation (40) is derived by

$$0 \leq fal(e)e \leq \delta^{\alpha-1}e^2 \tag{40}$$

Thus, there exists $\varphi_1 = 0, \varphi_2 = \delta^{\alpha-1}$ that satisfies Equation (39). Equation (40) can be expressed by

$$\varphi_1 e^2 \leq fal(e)e \leq \varphi_2 e^2 \tag{41}$$

According to Equation (28), Equation (31), and Equation (32), Equation (42) can be obtained as

$$G(s) = c^T(sI - \tilde{A})^{-1}\tilde{b} + \rho/s = \frac{q(s)}{p(s)} \tag{42}$$

where $p(s) = (\cos\phi\cos\theta)s(s + \frac{1}{\tau})^2(s + \frac{k_3}{m})(s + \frac{k_2\cos\phi\cos\theta}{b} + \frac{b}{k_1\cos\phi\cos\theta})$.

The solutions of characteristic equation $p(s) = 0$ are derived by

$$\begin{cases} \lambda_1 = -1/\tau \\ \lambda_2 = -k_3/m \\ \lambda_3 = -1/\tau \\ \lambda_4 = -k_2\cos\phi\cos\theta/b - b/(k_1\cos\phi\cos\theta) \\ \lambda_5 = 0 \end{cases} \tag{43}$$

If $\lambda_i \leq 0$, $i = 1, 2, \dots, 5$, then the condition (1) in Lemma 3.1 can be satisfied. τ, m, k_1, k_2, k_3 are all positive, and $\lambda_4 \neq 0$. That is to say, the condition (1) in Lemma 3.1 is satisfied when the Equation (37) is satisfied.

Equation (44) should be satisfied if the condition (2) in Theorem 3.1 holds.

$$\begin{cases} 1 + \varphi_1\mathrm{Re}[G(j\hat{\omega})] \neq 0 \\ \mathrm{p}(j\hat{\omega}) \neq 0 \end{cases} \tag{44}$$

According to Equation (44), set

$$\Omega^*_\varphi = \{\hat{\omega} : 1 + \varphi_1\mathrm{Re}[G(j\hat{\omega})] = 0 \text{ or } \hat{\omega} = 0\} \tag{45}$$

Only $\omega \in \Omega_\varphi$ is considered.

If Equation (37) is satisfied, then $p(s) + kq(s)$ is Hurwitz. According to the Nyquist stability theorem and Equation (41), it is derived by

$$\mathrm{Re}[G(j\omega)] \geq -\frac{1}{\varphi_1} \ \forall \omega \in \Omega_\varphi \tag{46}$$

According to Equation (46), Equation (38) can be expressed by

$$\varphi_2(\mathrm{Re}[G(j\omega)] + \varphi_1|G(j\omega)|^2) \geq -(1 + \varphi_1 \mathrm{Re}[G(j\omega)]) \tag{47}$$

where $\omega \in \Omega_\varphi$. Then, Equation (48) can be derived according to Equation (47).

$$\mathrm{Re}[1 + \varphi_1 G(-j\omega) + \varphi_2 G(j\omega) + \varphi_1\varphi_2|G(j\omega)|^2] \geq 0 \tag{48}$$

where $\omega \neq 0$, it is assumed that there exists an $\hat{\omega}$ satisfying Equation (48) if $\varphi_1 \neq 0$.

$$1 + \varphi_1 \mathrm{Re}[G(j\hat{\omega})] = 0 \tag{49}$$

Then Equation (48) can be simplified as

$$\mathrm{Re}[1 + \varphi_1 G(j\hat{\omega}) + \varphi_1^2|G(j\hat{\omega})|^2] \geq 1 \tag{50}$$

Substituting Equation (49) into Equation (50), we obtain

$$\varphi_1 \mathrm{Re}^2[G(j\hat{\omega})] + \varphi_1 \mathrm{Im}^2[G(j\hat{\omega})] - \frac{1}{\varphi_1} = \varphi_1 \mathrm{Im}^2[G(j\hat{\omega})] \geq 0 \tag{51}$$

Thus, $\omega \in \{\hat{\omega} : 1 + \varphi_1 \mathrm{Re}[G(j\hat{\omega})] = 0\}$ can satisfy Equation (49). Substituting Equation (42) into Equation (48), we obtain

$$\mathrm{Re}\left\{\left[1 + \frac{\varphi_1 q(-j\omega)}{p(-j\omega)} + \frac{\varphi_2 q(j\omega)}{p(j\omega)} + \frac{\varphi_1\varphi_2 q(-j\omega)q(j\omega)}{p(-j\omega)p(j\omega)}\right]|p(j\omega)|^2\right\} \geq 0 \tag{52}$$

where $\omega \in R$, the condition (2) in Lemma 3.1 can be derived by Equation (52).

The nonlinear system is frozen-time closed-loop stable according to Lemma 3.1.

Proof is complete. ■

4. Simulation

In this section, the simulations are conducted to verify the effectiveness of the presented robust PD-type trajectory tracking controller with ESO. Different scenarios are considered, including normal cases and cases under external disturbance. The parameters of the adopted quadrotor model are shown in Table 1. The parameters of the PD-type trajectory tracking controller are shown in Table 2.

Table 1. The parameter value of the quadrotor UAV.

The parameter	The value	The parameter	The value
m	1.06 kg	I_1	0.02
l	0.255 m	I_2	0.02
g	9.8 m/s^2	I_3	0.05
K_1	0.01	K_4	0.012
K_2	0.01	K_5	0.012
K_3	0.01	K_6	0.012

Table 2. The parameter value of PD-type trajectory tracking controller.

Case I		Case II	
The parameter	The value	The parameter	The value
k_{px}	5	k_{px}	10
k_{dx}	5	k_{dx}	10
k_{py}	5	k_{py}	20
k_{dy}	5	k_{dy}	25
k_{pz}	5	k_{pz}	35
k_{dz}	5	k_{dz}	35

Table 3. The values of the observer gains.

The observer gain	The value
β_1	100
β_2	950
β_3	6800

4.1. Simulation without disturbance

Case I: Set the desired position: $x_d = 5, y_d = 5, z_d = 10$. The system step response simulation is finish without disturbances. And the static position trajectory tracking response is obtained as follows.

As shown in Figure 6, the quadrotor can track the desired position trajectories within 3 s, and there are no overshoots in the transient state.

Figure 7 shows the quadrotor UAV three-dimensional static position trajectory tracking response curve. As shown in Figure 7, the three-dimensional tracking path is

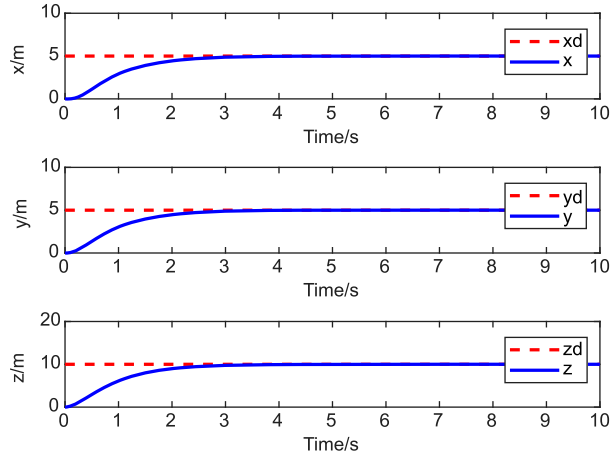

Figure 6. The static position trajectory tracking response.

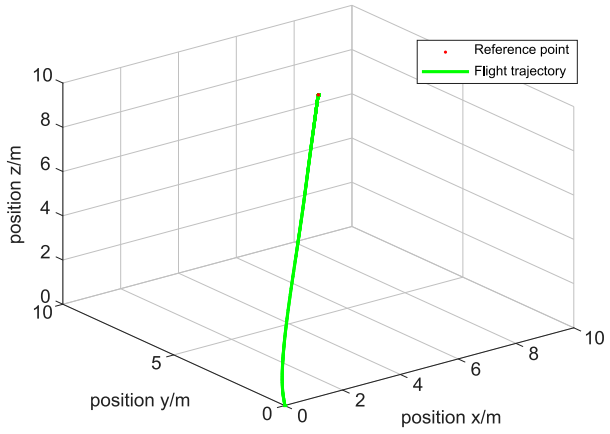

Figure 7. Three-dimensional static position trajectory tracking response.

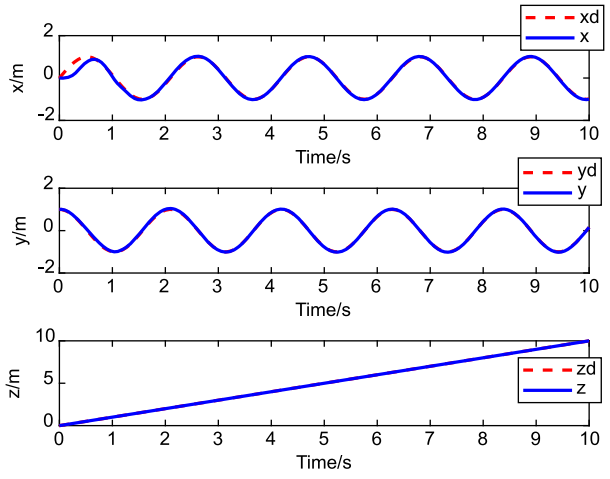

Figure 8. Dynamical position tracking response.

similar with the straight line from the initial point to the end.

Case II: Set the desired trajectory:$x_d = \sin(3t), y_d = \cos(3t), z_d = t$. At the moment, the quadrotor dynamical trajectory tracking is obtained as follows.

As shown in Figure 8, the quadrotor UAV tracks the desired dynamical position trajectory within 1 s. Three-dimensional dynamical tracking results are shown in 9. The simulation results validate the efficiency of the proposed PD trajectory tracking controller. The system can achieve fast response and high tracking precision without external disturbance.

4.2. Simulation with disturbance

In order to illustrate the disturbances rejection performance of PD trajectory tracking controller with the ESO, the external disturbances are considered in the simulation. The values of the observer gains are shown in Table 3.

Case I: The disturbance rejection performance is tested in the attitude loop. Set the desired angle: $\psi_d = 60^\circ$. The step response simulation is carried out with disturbances. Taking the yaw angle, for example, time-varying wind disturbance is added in yaw angle subsystem from 5 s to 7 s (9).

The estimated wind disturbance by the ESO is shown in Figure 10.

In Figure 10, the time-varying wind disturbance is estimated by the ESO, and the estimation error is small. In addition, there is the small-time delay between the real and estimated disturbance. The low-pass filter in Equation (23) may be the reason of the time delay.

The results of the anti-disturbance of in yaw angle are as follows in Figure 11.

As shown in Figure 11, the wind disturbance has great influence on the yaw angle when the PD controller is used alone in the system. And the peak of yaw angle is over 80° under the influence of disturbance. However, wind

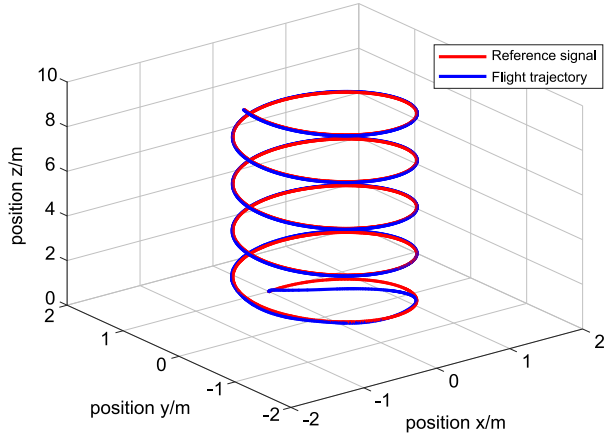

Figure 9. Three-dimensional dynamical tracking results.

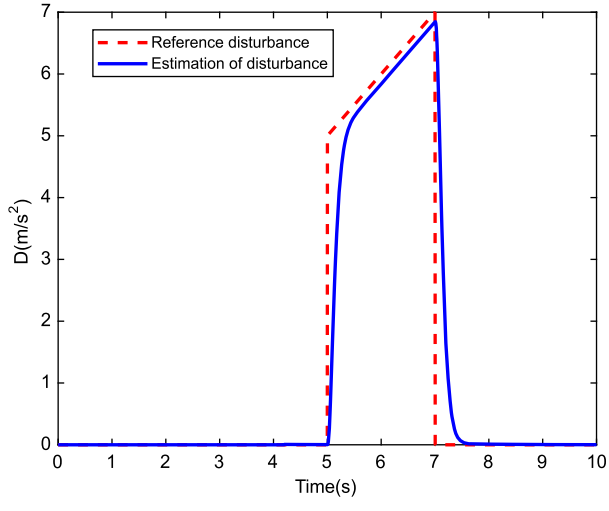

Figure 10. ESO disturbance estimation of yaw angle.

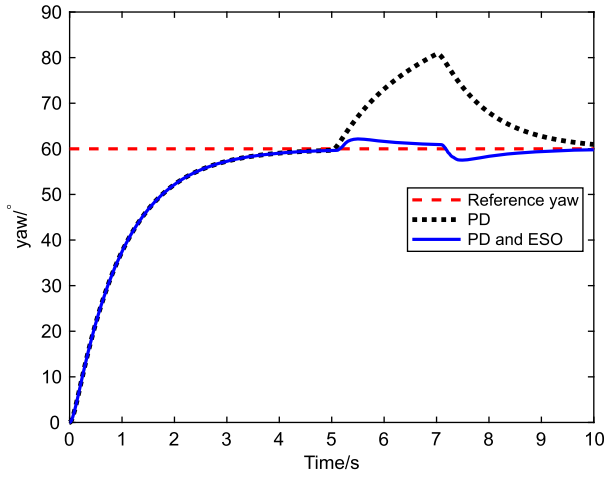

Figure 11. Yaw angle anti-disturbance response comparison.

disturbance causes the smaller changes on the yaw angle when the PD controller with the ESO is used to control the quadrotor UAV.

Case II: The disturbance rejection performance is tested in the outer loop of the system. Set the desired position: $x_d = 5, y_d = 5, z_d = 10$. The step response simulation is carried out with disturbances. Taking the z-axis for example, the wind disturbance is added in the z-axis subsystem from 5 s to 7 s.

The estimated wind disturbance by the ESO is shown in Figure 12.

The wind causes 3 m/s^2 accelerated speed disturbance to the z-axis subsystem. The disturbance is added at 5 s and disappeared at 7 s. In Figure 12, the wind disturbance is estimated by the ESO, and the estimation error is zero in steady-state.

The results of the anti-disturbance in the z-axis are as follows in Figure 13.

As similar with yaw angle anti-disturbance response, the wind disturbance has great influence on the z-axis

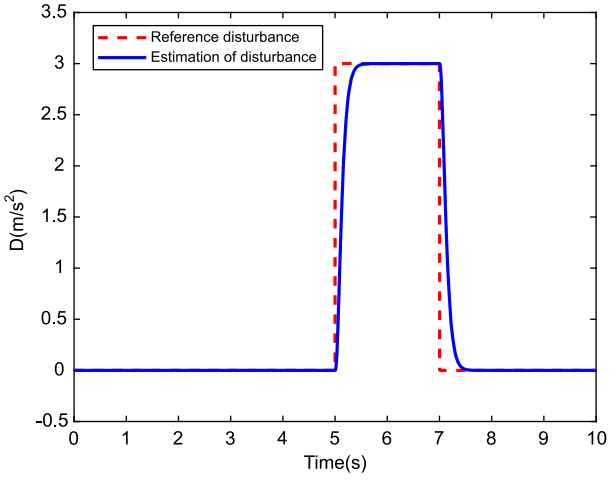

Figure 12. ESO disturbance estimation.

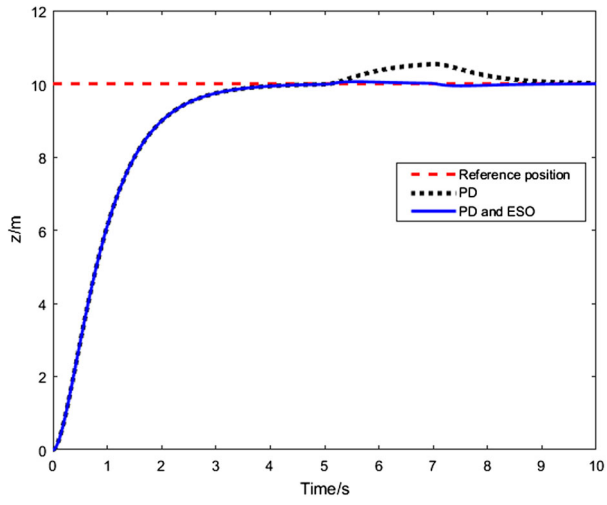

Figure 13. The z-axis anti-disturbance response comparison.

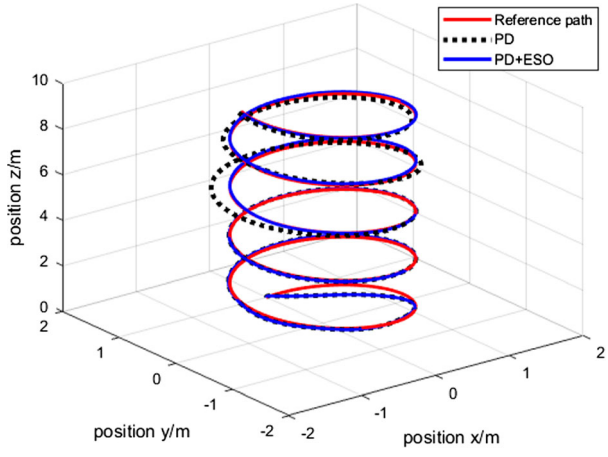

Figure 14. PD and ESO anti-disturbance dynamical tracking curve comparison.

when the PD controller is used alone in Figure 13. And the peak of the z-axis is over 10.5 m under the influence of disturbance. However, wind disturbance causes the smaller changes on the z-axis when the PD controller with the ESO is used to control the quadrotor UAV.

Case III: Set the desired trajectories are: $x_d = \sin(3t), y_d = \cos(3t), z_d = t$. The wind disturbance is added in the z-axis, and it is same as the situation in Case II. The results are as follows.

In Figure 14, there is the bigger tracking error when the PD controller is used alone. Meanwhile, the PD controller with the ESO can track the dynamical trajectory well.

5. Conclusion

The PD-type trajectory tracking controller with the ESO is proposed to improve the trajectory tracking performance

of the quadrotor UAV in the presence of the wind disturbance. The six-degree-of-freedom quadrotor UAV model is built, and the accuracy of the model is verified by the actual fight. In addition, the stability of the closed-loop system with the proposed controller is proved by the circle criterion. The simulation results indicate that the proposed method has the better tracking performance for the attitude and position than the PD tracking controller. And the wind disturbance can be estimated by the ESO with the small estimation error. In the future, the parameters uncertainty and faults will be considered for the trajectory tracking of the quadrotor UAV.

Disclosure statement

No potential conflict of interest was reported by the authors.

Funding

This work is supported by the National Nature Science Foundation under grant 61603220, 61333005, 61733009; the Research Fund for the Taishan Scholar Project of Shandong Province of China; SDUST Young Teachers Teaching Talent Training Plan under Grant BJRC20180503.

References

Bolandi, H., Rezaei, M., Mohsenipour, R., Nemati, H., & Smailzadeh, S. M. (2013). Attitude control of a quadrotor with optimized PID controller. *Intelligent Control and Automation*, *04*(3), 342–349.

Chen, F., Jiang, R., Zhang, K., Jiang, B., & Tao, G. (2016). Robust backstepping sliding-mode control and observer-based fault estimation for a quadrotor UAV. *IEEE Transactions on Industrial Electronics*, *63*(8), 5044–5056.

Chen, F., Lei, W., Zhang, K., Tao, G., & Jiang, B. (2016). A novel nonlinear resilient control for a quadrotor UAV via backstepping control and nonlinear disturbance observer. *Nonlinear Dynamics*, *85*(2), 1281–1295.

Chen, M., Tao, G., & Jiang, B. (2015). Dynamic surface control using neural networks for a class of uncertain nonlinear systems with input saturation. *IEEE Transactions on Neural Networks and Learning Systems*, *26*(9), 2086–2097.

Curran, P. (1993). Proof of the circle criterion for state space systems via quadratic Lyapunov functions — Part 2. *International Journal of Control*, *57*(4), 957–969.

Derafa, L., Benallegue, A., & Fridman, L. (2012). Super twisting control algorithm for the attitude tracking of a four rotors UAV. *Journal of the Franklin Institute*, *349*(2), 685–699.

Derafa, L., Ouldali, A., Madani, T., & Benallegue, A. (2011). Nonlinear control algorithm for the four rotors UAV attitude tracking problem. *The Aeronautical Journal*, *115*(1165), 175–185.

Dong, W., Gu, G. Y., Zhu, X., & Ding, H. (2014). High-performance trajectory tracking control of a quadrotor with disturbance observer. *Sensors and Actuators A: Physical*, *211*(5), 67–77.

Fernando, T., Chandiramani, J., Lee, T., & Gutierrez, H. (2011). *Robust adaptive geometric tracking controls on SO(3) with an application to the attitude dynamics of a quadrotor UAV*. Decision and Control and European Control Conference (Vol.413, pp. 7380–7385). IEEE.

Gan, Z., & Han, J. (2003). Lyapunov function of general Lurie systems with multiple nonlinearities. *Applied Mathematics Letters*, *16*(1), 119–126.

Jian, J., & Zhao, Z. (2015). Global stability in lagrange sense for bam-type Cohen–Grossberg neural networks with time-varying delays. *Systems Science & Control Engineering*, *3*(1), 1–7.

Kerma, M., Mokhtari, A., Abdelaziz, B., & Orlov, Y. (2012). Nonlinear H_∞ control of a quadrotor (uav), using high order sliding mode disturbances estimator. *International Journal of Control*, *85*(12), 1876–1885.

Li, M., Jing, W., Macdonald, M., & Mcinnes, C. R. (2011). Adaptive backstepping control for optimal descent with embedded autonomy. *Aerospace Science and Technology*, *15*(7), 589–594.

Li, J., Xia, Y., Qi, X., Gao, Z., Chang, K., & Pu, F. (2015). Absolute stability analysis of non-linear active disturbances rejection control for single-input–single-output systems via the circle criterion method. *IET Control Theory & Applications*, *9*(15), 2320–2329.

Lin, Q., Cai, Z. H., Wang, Y. X., Yang, J. P., & Chen, L. F. (2014). *Adaptive flight control design for quadrotor UAV based on dynamic inversion and neural networks*. Third International Conference on Instrumentation, Measurement, Computer, Communication and Control, 1461–1466.

Mandel, Y., & Weiss, G. (2015). Adaptive internal model-based suppression of torque ripple in brushless dc motor drives. *Systems Science & Control Engineering*, *3*(1), 162–176.

Mi, Y., Fu, Y., Li, D., Wang, C., Loh, P. C., & Wang, P. (2016). The sliding mode load frequency control for hybrid power system based on disturbance observer. *International Journal of Electrical Power & Energy Systems*, *74*(8), 446–452.

Sandiwan, A. P., Cahyadi, A., & Herdjunanto, S. (2017). Robust proportional-derivative control on SO(3) with disturbances compensation for quadrotor UAV. *International Journal of Control Automation & Systems*, *15*(4), 1–14.

Shao, X., Liu, J., Cao, H., Shen, C., & Wang, H. (2018). Robust dynamic surface trajectory tracking control for a quadrotor UAV via extended state observer. *International Journal of Robust and Nonlinear Control*, *28*(7), 2700–2719.

Sheng, L., Zhang, W., & Gao, M. (2014). Relationship between Nash equilibrium strategies and H-2/H-infinity control of Stochastic Markov jump systems with multiplicative noise. *IEEE Transactions on Automatic Control*, *59*(9), 2592–2597.

Song, Y., Wang, Y., & Wen, C. (2016). Adaptive fault-tolerant pi tracking control with guaranteed transient and steady-state performance. *IEEE Transactions on Automatic Control*, *62*(1), 481–487.

Wang, C., Chen, Z., Sun, Q., & Zhang, Q. (2016). *Design of PID and ADRC based quadrotor helicopter control system*. Control and Decision Conference (pp. 5860–5865). IEEE.

Wang, C., Li, X., Guo, L., & Li, Y. W. (2014). A nonlinear-disturbances-observer-based DC-bus voltage control for a hybrid AC/DC microgrid. *IEEE Transactions on Power Electronics*, *29*(11), 6162–6177.

Wang, P., Wang, J., Bu, X., Luo, C., & Tan, S. (2017). Adaptive fuzzy back-stepping control of a flexible air-breathing hypersonic vehicle subject to input constraints. *Journal of Intelligent & Robotic Systems*, *35*(9), 1–18.

Zhang, N., Gai, W., Zhang, G., & Zhang, J. (2018). An active disturbances rejection control guidance law based collision avoidance for unmanned aerial vehicles. *Aerospace Science and Technology*, *77*, 658–669.